

On the rational design of mesoporous silica humidity sensors

Máté Füredi^a, Alberto Alvarez-Fernandez^a, Maximiliano Jara Fornerod^a, Bálint Fodor^b and Stefan Guldin^{a,*}

^aDepartment of Chemical Engineering, University College London, Torrington Place, London, WC1E 7JE, United Kingdom.

^bSemilab Semiconductor Physics Laboratory Co. Ltd, 4/A Prielle K. str., 1117 Budapest, Hungary

*Email: s.guldin@ucl.ac.uk

Abstract

Mesoporous silica is commonly used as matrix for humidity sensors, which operate on the principle of relative humidity-dependent water uptake and read-out by resistive or capacitive means. Although numerous studies have been dedicated to improving the sensing performance, the effect of pore structure on sensing behaviour has not been systematically investigated so far. Herein, we showcase the effects of pore size and porosity on resistive sensing behaviour in the 0.5-85% relative humidity (RH) range. We employed evaporation-induced self-assembly (EISA) in combination with sol-gel chemistry to fabricate well-defined mesoporous silica thin films with high degree of structural control. Material architectures with pore sizes of 3 to 15 nm and porosities of 40 to 70% were rationally designed by using structure directing agents (SDAs) with increasing molecular weight and tuning the silica to SDA ratio. We found that a combination of pore size of 15 nm and 70% porosity showcases a particularly high sensitivity ($\sim 10^4$ times change in resistance) in the measured range, with quick response and recovery times of 3 and 9 seconds, respectively. Across the various sensors, we identified a clear correlation between the pore size and the linear RH sensing range. Additionally, increasing the porosity while retaining the pore size, yields better overall sensitivity across the range. Our findings may serve as guidelines for developing broad spectrum high-performance mesoporous sensors and for sensors specifically engineered for optimal operation in specific RH ranges.

Keywords: block copolymers, ellipsometric porosimetry, humidity sensor, mesoporous silica, self-assembly, thin films.

1. Introduction.

Sensing the relative humidity is a key feature in applications where moisture variation has either an effect on the desired performance (agriculture [1,2], food processing [3], electronics [4], corrosion [5]), or where the user comfort benefits from humidity control (automotive [6], aviation [7], smart home [8], healthcare [9], and space vehicles industries [10]). Humidity sensors with wide detection range, high sensitivity and selectivity, small hysteresis, rapid response and recovery times, coupled with low fabrication cost, are the focus of research nowadays [11]. Typically, humidity sensing relies on a change in the physical properties of a material system when interacting with different amounts of gas phase water molecules, for example, changes in the impedance [12,13], piezoelectricity [14], refractive index [15], Bragg peak [16], capacitance [17,18] or electrical resistance [19,20] of the system. The last two examples, i.e., resistive and capacitive sensors, represent the most extensively used sensors in industrial applications due to the low cost and energy consumption, and the ease of fabrication and integration with electronic circuits. However, they also display lower accuracy, compared to optical humidity sensors [11,21].

Besides full range sensing, there is emerging attention towards sensors with exceptionally high sensitivity in specific ranges. Relative humidity (RH) is often controlled to be within 40% and 60% in indoor public spaces for comfort and health effects [22], making this RH range of particular interest for commercial sensors. On the other hand, some processes, such as fuel cell operation are carried out in a tightly controlled low RH environment [23]. Engineering humidity sensors for maximum performance in a narrow range enables better accuracy in monitoring and controlling the RH in such applications. Conventional humidity sensors, often operating on capacitance changes in polymers are widely available

at low cost. However, their low sensitivity, limited range, and slow response/recovery times make them unsuitable for demanding modern industrial applications mentioned above [11]. The integration of nanostructured materials, such as nanoporous polymers [24], metal-oxides [25–29] and silica [29–34], enabled the development of wide-range, high-performance resistive and capacitive humidity sensors. These sensors can exhibit sensitivities over 4 orders of magnitude resistance/impedance change (ΔR or ΔZ) between 11% and 98% RH [28,35–37]. The improvement in sensitivity of mesoporous materials compared to their nonporous counterparts [38] is related to the fact that mesoporous materials can adsorb atmospheric humidity well below saturation, changing the electrical properties of the sensing layer (see schematic in **Figure S1**). The sensing mechanism typically follows four consecutive steps with increasing relative humidity, which depend on pore size and surface functionalisation: micropore filling, monolayer formation, multilayer adsorption, and finally capillary condensation. In this context, the Kelvin equation provides a relationship between the RH at which capillary condensation occurs and the mesoscale pore size (2 to 50 nm) [39]. Additionally, high accessible porosity and large surface area facilitate the protonic conduction of water referred to as Grotthuss mechanism [40].

While multiple fabrication methods have been studied to obtain porous inorganic materials for humidity sensing, such as etching of silicon [41,42], aluminium[43], and graphene [44], most of these top-down approaches face challenges with respect to reproducibility, cost-effectiveness, and scalability. In contrast, the use of sol-gel chemistry enables facile bottom-up methods for preparing mesoporous silica with controlled architectures. Structure directing agents (SDAs), such as surfactants [45] and block copolymers (BCP) [46] can be utilized to prepare mesoporous materials with tuneable porosities, pore sizes and pore morphologies [47–51], via co-assembly with inorganic precursors.

Mesoporous silica is one of the most versatile matrix materials for research of high-performance humidity sensors due to its low cost, ease of preparation, high surface area, and surface silanol groups, which can be utilized for functionalization [52]. Since the first studies introducing cetyltrimethyl ammonium bromide (CTAB) and poly(ethylene oxide)-

poly(propylene oxide)-poly(ethylene oxide) (PEO-*b*-PPO-*b*-PEO) triblock copolymer templated mesoporous silica films as humidity sensors in the early 2000s [38,53], this fabrication route has become well established in the field of resistive humidity sensors. A substantial amount of recent research has been devoted to enhancing sensing performance of such matrices with dopants, such as Li [30,31], Na [36], K [33], Ag [54], or with nanocomposites, such as TiO₂ [35], and WO₃ [32,55].

PEO-*b*-PPO-*b*-PEO is the most commonly used BCP for co-assembly, typically as commercially available P123, or PF127. Recent works have, however demonstrated the preparation of mesoporous materials containing large mesopores (>10 nm) with diblock high- χ (highly amphiphilic) BCP SDAs, such as poly(isobutylene)-block-poly(ethylene oxide) (PIB-*b*-PEO) [56], poly(isoprene)-block-poly(ethylene oxide) (PI-*b*-PEO) [57] or hydrogenated poly(butadiene)-block-poly(ethylene oxide) (PHB-*b*-PEO) [46].

To this end, the effect of mesoporous structure on sensing behaviour has not been systematically studied yet. In most cases, a single SDA was used for the synthesis of mesoporous silica matrices without a detailed study on the influence of pore structure. In studies considering multiple SDAs, performance differences were attributed to the structural characteristics [38]. However, a lack of suitable tools to characterise the material architecture has prevented the validation of this hypothesis. Furthermore, the applicability of larger molecular weight and high- χ BCPs as SDAs for silica humidity sensors has not been investigated to date, preventing to explore a wider range of porosities and pore sizes. In response, this work aims to establish a detailed structure-function relationship between pore architecture of mesoporous silica thin films and their humidity sensing behaviour by conducting a systematic study of multiple parameters. We first fabricate mesoporous silica thin films using different SDAs to control the pore size and porosity of the material. We then employ ellipsometric porosimetry and the electrical resistance measurements of the films to evaluate the response upon RH change. Finally, we demonstrate how independent manipulation of mesopore size and porosity enables tuneable sensitivity across different RH ranges.

2. Experimental.

2.1 Chemicals: All chemicals were used as received without further purification. Tetraethyl-orthosilicate (TEOS, >99%) was purchased from Sigma. Ethanol (99.8%) was purchased from Fischer Scientific. Ultrahigh purity MilliQ water was used where stated. Concentrated hydrochloric acid (37%) was purchased from Merck. CTAB (>99%) was purchased from Sigma. Powder form PEO₁₀₆-PPO₇₀-PEO₁₀₆ (PF127) and PEO₂₀-PPO₇₀-PEO₂₀ (P123) were purchased from Sigma. PIB₃₉-PEO₃₆ was supplied by BASF.

2.2 Preparation of mesoporous silica materials: We prepared mesoporous silica materials using the following SDAs (see **Table 1**):

2.2.1- CTAB/compound templating: 2.08 g TEOS was mixed with 2.218 ml ethanol, with the subsequent dropwise addition of 0.901 ml (pH=1.33) hydrochloric acid. This sol was aged at 40°C for 4 hours before adding sufficient CTAB/EtOH solution to reach 0.14 CTAB/TEOS molar ratio (as reported elsewhere [58]). P123 as a co-surfactant was added in this step in a 0.02 P123/TEOS molar ratio. The combined use of P123 and CTAB was reported before to possess improved properties [59]. Because of the very high (~35) CTAB/P123 molar ratio used in our case, the thus prepared film will be denoted from here on as 'SiO₂-CTAB'.

2.2.2- PEO-*b*-PPO-*b*-PEO templating: 4.5 g TEOS was mixed with 2.363 ml ethanol. 2.138 ml 10 mM hydrochloric acid was added dropwise to create a precursor sol with nominally 1000 mg/ml inorganic silica concentration. The sol was stirred at room temperature for 3 hours before pipetting and transferring 0.360 ml to a new vial and mixing with the ethanolic solution of either 0.900 ml (50 mg/ml) P123 or 0.576ml (103.6 mg/ml) PF127. The thus prepared films will be denoted from here on as 'SiO₂-P' for the P123 templated material or 'SiO₂-PF' for PF127 templated material.

2.2.3- PIB-*b*-PEO templating: 4.5 g TEOS was mixed with 2.363 ml ethanol. 2.138 ml 10 mM hydrochloric acid was added dropwise to create a precursor sol with nominally 1000 mg/ml inorganic silica concentration. The sol was stirred at room temperature for 3 hours before pipetting and transferring 0.360 ml to a new vial and mixing with the ethanolic

solution of 0.636 ml (50 mg/ml) PIB-*b*-PEO for a 15% nominal organic mass ratio. Various template/silica sol ratios were prepared by modifying the PIB-*b*-PEO solution added (the nominal organic/inorganic mass varied from 10% to 35%). The thus prepared films will be denoted from here on as ‘SiO₂-PIB10’, ‘SiO₂-PIB15’, ‘SiO₂-PIB25’ and ‘SiO₂-PIB35’ based on the nominal SDA content used.

Table 1 Comparison of structure directing agents used for sol-gel synthesis

Name of SDA	Formula	M _w (g/mol)	wt% PEO
CTAB	CH ₃ (CH ₂) ₁₅ -N(CH ₃) ₃ Br	364.45	N/A
P123	PEO ₂₀ -PPO ₇₀ -PEO ₂₀	5800	30.5
PF127	PEO ₁₀₆ -PPO ₇₀ -PEO ₀₆	12600	69.7
PIB-<i>b</i>-PEO	PIB ₃₉ -PEO ₃₆	4850	41.7

2.3 Fabrication of transparent humidity sensors

After the silica sols were combined with the various SDA solutions, the mixtures were immediately spin-coated at 5000 rpm onto silicon and interdigitated transparent conducting electrode (indium tin oxide) coated glass substrates (Ossila Ltd, 20 x15 mm, electrode thickness: 100 nm, distance between electrodes 50 μm) respectively. For removing the organic SDAs and the complete condensation of the inorganic precursor, the samples were calcined in a muffle furnace at 450 °C for 30 mins (5°C /min ramping speed).

2.4 Humidity sensing measurements

The change in electrical resistance of the sensors upon exposure to humidity was measured by a Keithley 2450 source measure unit (SMU) using a bias voltage of 10 V with 10 s wait time. 40 individual RH steps were set in the range between 0.5%–85% by humidity chamber with controllable N₂ and air with saturated level of H₂O vapour (dry and wet gas) intake. Prior to resistance measurements, samples were treated with oxygen plasma for 300 s to remove residual organic contaminants inside the pores. Samples were subjected to 30 minutes of constant bias voltage before commencing measurements.

2.5 Material Characterization

Ellipsometric porosimetry (EP) measurements were carried out on a Semilab SE-2000 variable angle spectroscopic ellipsometer (within the spectral range of 300 to 900 nm) with humidity and vacuum chamber extensions for measurements with water and methanol adsorptives respectively. All ellipsometric data analysis was performed with Semilab's SEA software using Cauchy dispersion model fitting. For the environmental ellipsometric porosimetry (EEP) and vacuum ellipsometric porosimetry measurements, thin films spin-coated from the same sol onto silicon wafers were studied due to the better reliability of obtaining ellipsometric spectra of thin films deposited on absorbing substrates.

During ellipsometric porosimetry measurements, ellipsometric spectra were recorded stepwise at 30 P/P_0 steps (in the range between 0.5%–100%) to obtain the adsorption and desorption isotherms from the fitted refractive index values. The set relative humidity doses were achieved via the integrated closed humidity chamber with controllable nitrogen and air with saturated level of H_2O vapour (dry and wet gas) intake. The modified Kelvin-equation was used to obtain mesopore size distribution information as described previously [60]. Measurements with methanol adsorptive were analogously carried out in a vacuum chamber connected through a proportional valve to a vessel filled with methanol enabling precise control of relative adsorptive pressure. Prior to all EP measurements, samples were treated with oxygen plasma for 300 s to remove residual organic contaminants inside the pores.

Lorentz-Lorenz effective medium approximation (EMA) was be utilized to model the refractive index of porous solids partially filled with air and adsorptive molecules. Ellipsometric spectra acquired at different relative pressures of the adsorptive were used to construct volume adsorbed isotherms. Porosity was calculated using the Lorentz-Lorenz EMA for the adsorptive filled porous layer at $P/P_0=1$, while the modified Kelvin-equation enabled pore size distribution calculations [61]. Specific surface area was derived via the classical BET-fitting on the obtained isotherms [61–63].

Atomic force microscopy (AFM) was used to capture the surface morphology of prepared mesoporous silica samples. AFM images were obtained on a Bruker Dimension Icon

atomic force microscope with a SCOUT350 (Nunano, UK) probe (nominal tip radius 5 nm) in tapping mode.

Grazing incidence small angle X-ray scattering (GISAXS) measurements were performed at the Centre de Recherche Paul Pascal (CRPP) at Université de Bordeaux using a high-resolution X-ray spectrometer Xeuss 2.0 (Xenoxs) operating with radiation wavelength of $= 1.54 \text{ \AA}$. 2D scattering patterns were collected using a PILATUS 300K Dectris detector with a sample-to-detector distance of 1188 mm. The beam centre position and the angular range were calibrated using a silver behenate standard sample. GISAXS data analysis was accomplished with the FitGISAXS software [64].

3. Results and discussion

As previously introduced, two critical parameters in the fabrication of high-performance mesoporous humidity sensors are pore size and porosity. In order to establish a comprehensive and detailed study on the influence and impact of both parameters for the humidity sensing application, fine control over pore size (via sol-gel synthesis with different molecular weight (M_w) SDA) and porosity (via tuning SDA:inorganic ratio) has been explored (**Figure 1A**). In a subsequent step, the humidity-sensing performance of the different mesoporous thin films was studied following methodology show in **Figure 1B**.

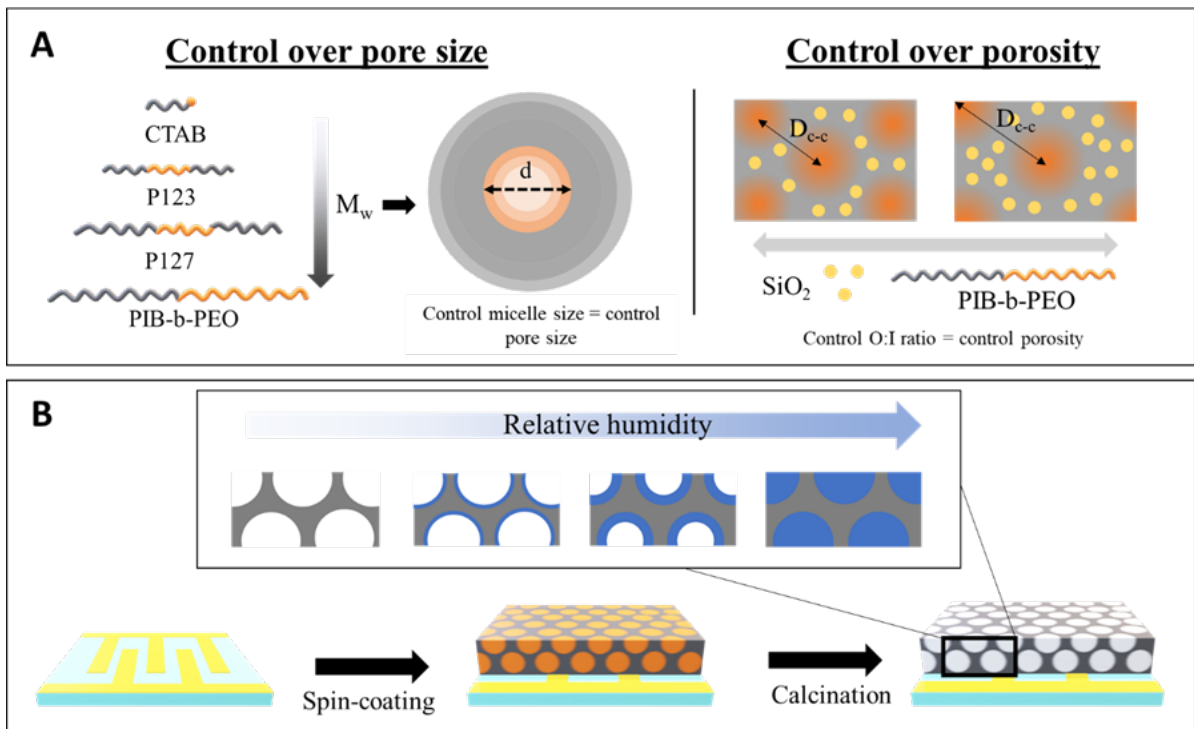


Figure 1. A) Strategy towards the preparation of mesoporous humidity sensing layers with tuneable pore size and porosity (M_w : molecular weight, d : pore diameter, D_{c-c} interpore distance, O:I ratio: organic/inorganic ratio). B) Strategy of humidity sensing based on capillary condensation on the mesoporous films.

3.1.- Influence of pore size.

3.1.1.- Fabrication of mesoporous thin films with controllable pore sizes.

Different SDAs, namely CTAB, P123, PF127 and PIB-b-PEO, were used in the fabrication of mesoporous thin films with tuneable pore sizes. Due to the variation in molecular weight (M_w) between the different SDAs employed, inorganic mesoporous architectures with increasing pore dimensions were obtained. AFM topographic micrographs presented in **Figure 2** confirm the presence of a porous structure in all samples. However, limited information on pore sizes and porosity can be derived from samples obtained by the lower M_w SDAs (CTAB and P123), which may be related to the resolution limit of the used tip and reveals some restrictions of surface imaging techniques in the precise characterization of mesoporous architectures[61].

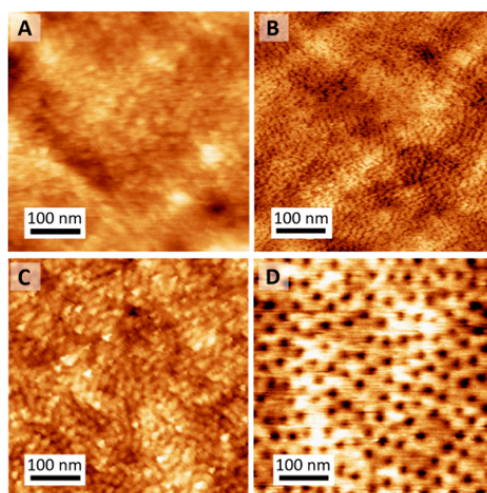


Figure 2. AFM micrographs of SiO₂-CTAB (A), SiO₂-P (B), SiO₂-PF (C) and SiO₂-PIB15 (D) films.

In order to obtain precise information across the full range of porous architectures, EEP was chosen as the standard characterization technique. **Figure 3A-D** presents the adsorption - desorption isotherms obtained by EEP of all mesoporous silica materials created using different SDAs. The pore size distribution graphs corresponding to the volume adsorbed isotherms are shown in **Figure 3E-H**. Increases in the pore dimensions, related to the increment in the diameter of micelles formed by SDAs in solution allowed pore size (diameter, D_{pore}) tuning between 3 and 15 nm, while keeping the porosity constant ($47\% \pm 3\%$). All adsorption isotherms, corresponding to the four different SDA templated films, show sharp increases in adsorbed volumes at characteristic relative pressure values, which is attributed to the capillary condensation of water in the mesopores. A summary of the structural properties obtained by EEP is shown in the SI Table S1, including respective film thicknesses and refractive indices. Notably, the total porosity and open porosity of the materials were in high correlation, showing the good accessibility of prepared porous architectures towards water. As expected for mesoporous materials, the desorption curves showcase different behaviour compared to adsorption. This hysteresis effect is usually attributed to the dimensions of interconnections between mesopores, however, the very late desorption in SiO₂-PF, and SiO₂-PIB15 templated silica may also be caused by cavitation [65].

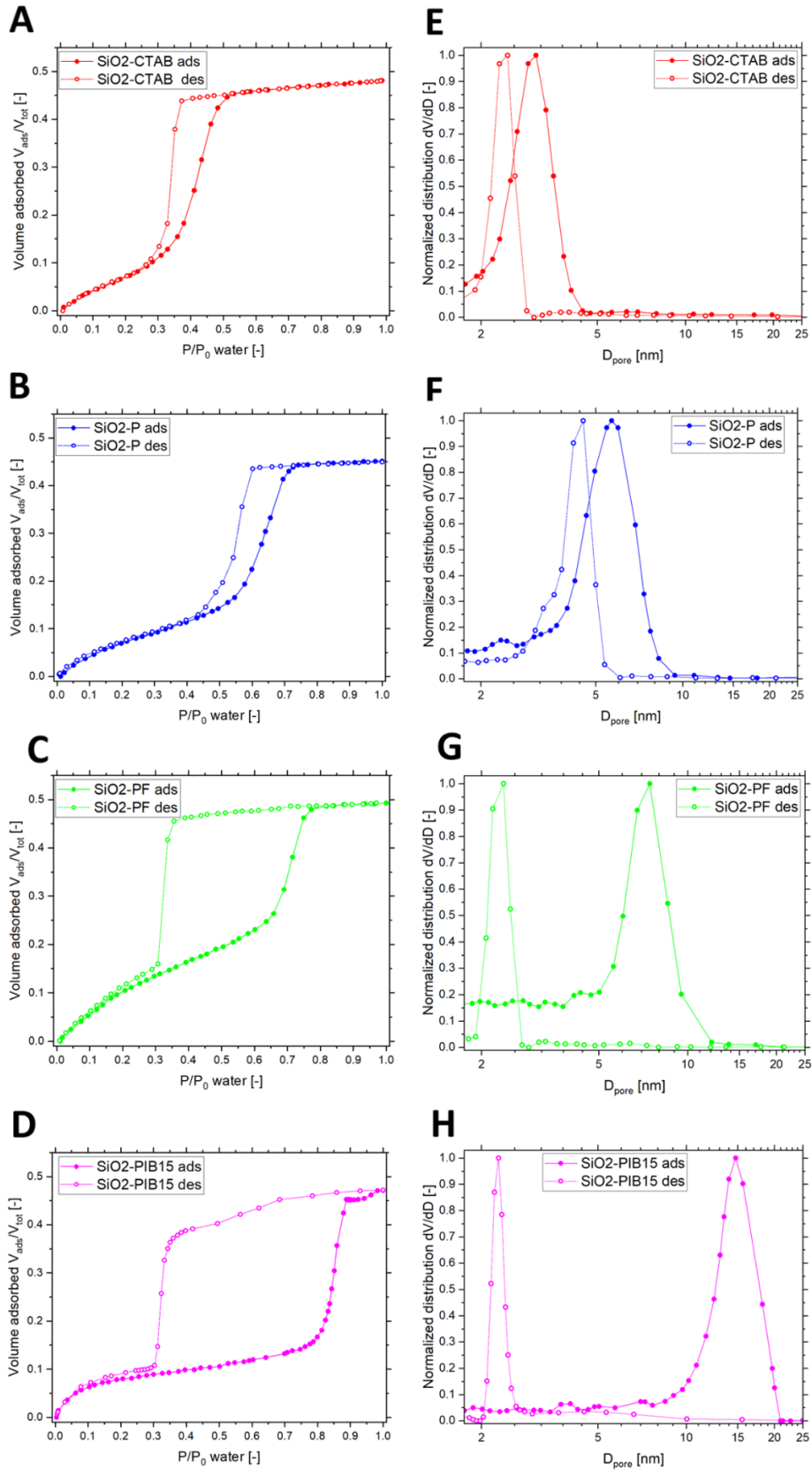


Figure 3. Volume adsorbed/desorbed ratio of water acquired by environmental ellipsometric porosimetry (A-D) and corresponding calculated pore diameter distributions (E-H) for SiO₂-CTAB (A, E), SiO₂-P (B, F), SiO₂-PF (C, G) and SiO₂-PIB15 (D, H) films

Since EEP uses water as adsorptive at room temperature instead of N₂ at 77K in the commonly employed BET-porosimetry technique or bulk powders, it can present more relevant results for humidity sensors. Furthermore, the optical nature of the technique enables the study of porous films ranging from nm to μm thickness in a non-destructive and reliable way through acquiring refractive index, extinction coefficient and thickness information based on the change of polarization of the reflected light [66]. Since neither volumetric nor gravimetric measurement of the adsorptive is not carried out, the accuracy of measurement is independent of the quantity of the studied adsorbent film, which makes it especially suitable for thin film humidity sensing layers.

3.1.2 Humidity sensing characteristics – effect of pore size on dynamic range

To investigate the influence of pore size in the humidity sensor response, previously fabricated mesoporous thin films, with similar porosity and increasing pore size (SiO₂-CTAB, SiO₂-P, SiO₂-PF, and SiO₂-PIB15) were studied. Changes in the electrical resistance of these sensing layers upon humidity variation are shown in **Figure 4A-D** and **Figure S2A**. We observed monotonously decreasing resistance with the increase of relative humidity for all four sensors, where the resistance of the sensors at 85% RH was approximately 10⁴ times smaller than at 0.5% RH. This 4 orders of magnitude change in resistance is comparable to the 3 – 5 orders of magnitude sensitivity (ΔR across full measured RH range) reported for other high-performance mesoporous silica-based sensors in the past 5 years [52,55,67,68]. All mesopore architectures displayed significant differences in their behaviour across specific sections of the measured humidity range (0.5-85%), as visible in **Figure 4**. In contrast to the common benchmarking of humidity sensors by measuring their resistance at 5 or 6 points of RH (e.g., 11, 33, 54, 78, 98%) via saturated salt solutions [69–71], we utilized a humidity chamber, in which the environment (RH) is continuously controllable across the spectrum without the need to remove the benchmarked sensor between measurement steps. The described setup enabled us to acquire resistance data at over 30 points between 0.5% and 85% RH for in-depth analysis. With each measurement cycle (corresponding to a respective sensor), we aimed to

establish a near-continuous function of the resistance-relative humidity relationship, referred to as ‘sensitivity plot’. While linear response (i.e., near constant slope of $\log R/RH$ function) of the sensors is generally deemed favourable for accurate sensing, another attribute that is considering is the location of the RH range where a sensor exhibits the largest slope of resistance decrease. For quantifying this, -local sensitivity ($d(\log R)/d(RH)$)- is defined as the first derivative of sensor resistance vs RH (see SI **Figure S2**) [72]. This allows for a numerical comparison between sensing behaviours at different segments of the RH range.

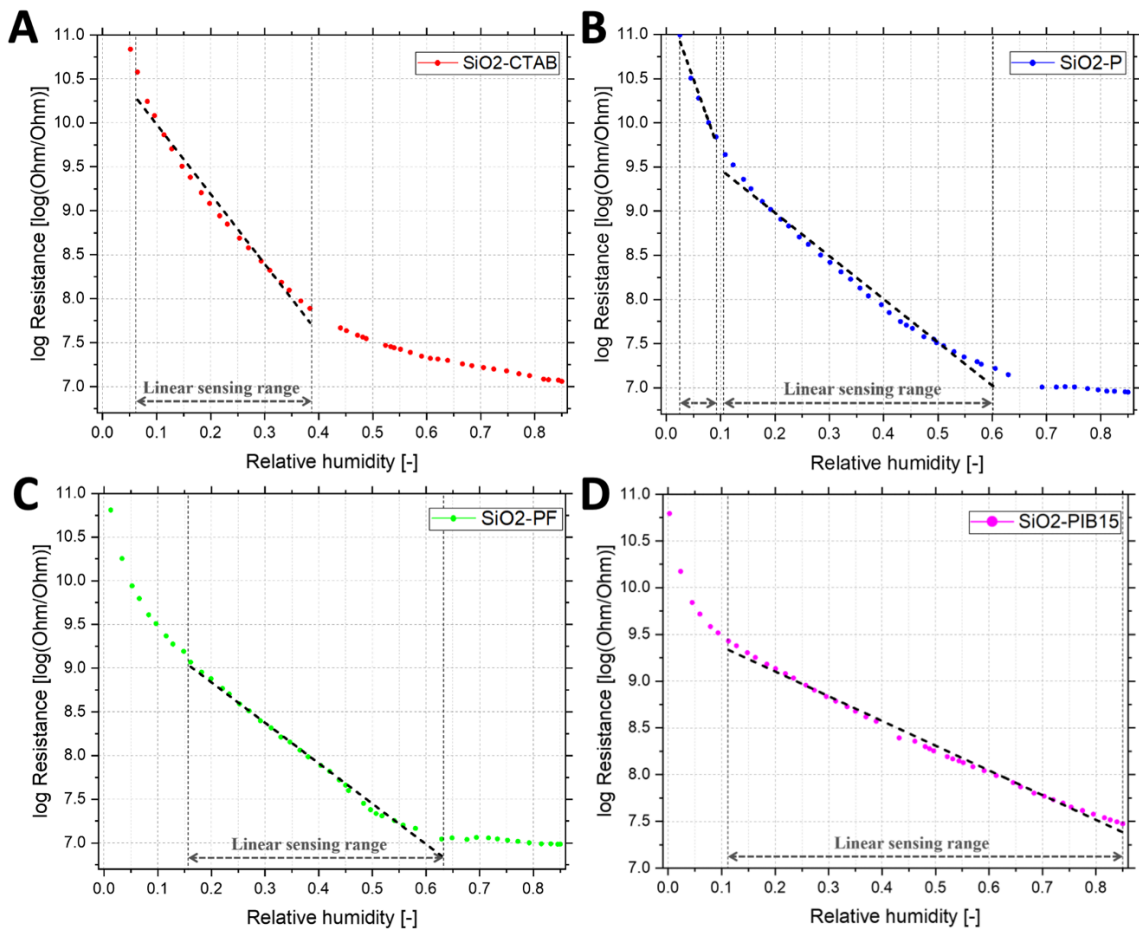


Figure 4. Sensitivity plots for adsorption of sensors SiO2-CTAB (A), SiO2-P (B), SiO2-PF (C) and SiO2-PIB15 (D), all possessing $47\% \pm 3\%$ porosity, with linear fit in the linear sensing ranges identified.

SiO₂-CTAB exhibited a pronounced slope (higher local sensitivity) until 40% RH (see **Figure 4A**) with relatively good linearity, while the measured sensitivity significantly decreased after 40% RH (see **Figure 4B** and **Figure S2B**). In comparison, SiO₂-P exhibited near-perfect linear relationship between 10% and 60% RH (see **Figure 4B**) with limited sensitivity beyond this point. This material, also known as SBA-15 has been regularly studied for mesoporous humidity sensing applications [30,31,33,38]. This ‘sensitivity cut-off’ – outlined in the two examples above – coincided with the saturation of mesopores with water during EEP measurements. As shown in **Figure 3**, very little H₂O was adsorbed at higher RH than 45% in the small mesopores (~3nm) of the SiO₂-CTAB film, since most of them were completely filled at this point. The same explanation holds true for the larger mesopores (~7nm) in SiO₂-P material above 65% RH.

As shown in **Figure 4C/D**, Sensor SiO₂-PF exhibited similar behaviour as sensor SiO₂-P with a larger decrease of resistance at very low RH (<5%), while sensor SiO₂-PIB15 displayed linear slope until high RH (85%) after a steep decline in resistance at very low RH (<5%). One possible explanation for the steep decline in resistance at low RH in the case of sensors SiO₂-PF and SiO₂-PIB15 is the presence of micropores that adsorb water at such low relative pressure range to form a conductive pathway in the films for ‘proton hopping’ even prior to monolayer formation. Previous reports have described the formation of micropores in other block-copolymer templated silica materials, which was attributed to hydrophilic PEO chains penetrating the silica matrix during film formation [73–75]. While PF127, P123 and PIB-*b*-PEO are all block copolymers with PEO components, it is worth noting that PF127 displays a higher volume fraction of ethylene-oxide compared to P123 (see **Table 1**). Notably, we detected a higher microporous adsorption in the cases of sensors SiO₂-PIB15 and SiO₂-PF when compared to sensors SiO₂-CTAB and SiO₂-P, which further supports our hypothesis (see **Figure 3** below 0.15 P/P₀). Based on these results high- χ BCP templated silica sensors can be deemed superior for broad spectrum relative humidity sensing, as they enable the incorporation of larger mesopores (>10 nm) to the matrix. One example of these, PIB-*b*-PEO templated silica (SiO₂-PIB15) showcased the widest linear range (see **Figures 4D** and **S2**) and the largest

low (<5%) RH sensitivity out of the 47%±3% porosity sensors investigated in this section, owing to its hierarchical structure of micropores and large mesopores.

3.1.3.- Humidity sensing characteristics – influence of pore size on response and recovery times

Response and recovery times were calculated based on fitting described in the Supporting Information. Response times of ~3-4 seconds were observed in all sensors (**Table 2**). For sensors SiO₂-CTAB and SiO₂-P, we observed rapid recovery times of 7 s and 5 s, respectively. In comparison, sensors SiO₂-PF and SiO₂-PIB15 exhibited much slower recovery (30 s and 53 s, respectively). Based on changes in pore size alone, no correlations could be drawn regarding recovery behaviour, indicating a more significant effects of other parameters such as micro- and mesoporosity. These are discussed in detail in Section 3.2.3.

3.2.- Influence of porosity

3.2.1.- Fabrication of mesoporous thin films with controllable porosities.

To study the effect of porosity on the humidity response, we prepared films with similar pore size and different porosity. PIB-*b*-PEO was selected as the sole SDA due to the promising performance of sensor SiO₂-PIB15 discussed previously. **Figure 5** exhibits isotherms of PIB-*b*-PEO templated silica sensors prepared using varying template:material (organic:inorganic) mass ratios. The similarity of isotherms confirmed that it was possible to tune the final porosity of the film (between 40% and 69%) while keeping the pore size nearly constant. GISAXS measurements (shown in **Figure S4**) confirm the decrease of centre-to-centre pore distances with increasing SDA content, indicating a thinner pore wall thickness for the more porous sensors.

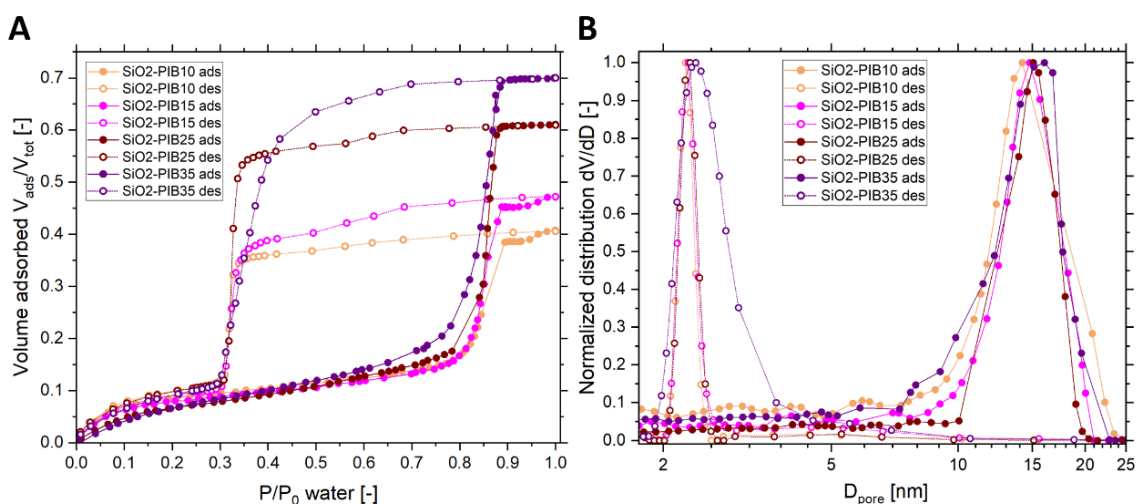


Figure 5. Volume adsorbed/desorbed ratio of water acquired by environmental ellipsometric porosimetry (A) and calculated pore size distribution (B) of SiO₂-PIB films prepared from precursor sols containing nominally 10%, 15%, 25% and 35% organic SDA weight ratios

3.2.2.- Humidity sensing characteristics – effect of porosity on dynamic range

To study the effect of porosity in the humidity response of the sensors, SiO₂-PIB samples with tuned porosity values, prepared in previous section, were investigated. The sensitivity and linear range is shown in **Figure 6A-D** for sensors SiO₂-PIB10, SiO₂-PIB15, SiO₂-PIB25 and SiO₂-PIB35. We observed that the obtained microporosity, i.e. pores <2 nm, was inversely proportional to the amount of SDA used in the fabrication of the films (**Figure 5**). To verify this observation, we characterised the samples using vacuum EP with methanol as adsorptive (see **Figure S5**). Based on methanol adsorption, 10 w% of SDA resulted in ~9.5 vol% microporosity, while using 35w% SDA led to only ~6.5 vol%. This phenomenon could be the result of higher material:template ratio of the less porous films. Previous studies have observed increased microporosity with higher material:template ratio in the case of PEO-*b*-PPO-*b*-PEO templated silica. This effect was attributed to stress-induced defects in pore walls caused by PEO chains, which give way to more micropores (i.e. defects) in the case of lower porosity (higher wall thickness) [76]. Our results highlight a similar phenomenon in high- χ BCP templated silica humidity sensors, which also influences sensing behaviour in the <5% RH range. This is in line with the aforementioned GISAXS measurements (**Figure S4**), providing evidence of increasing

wall thickness for sensors prepared using lower SDA content. While the local sensitivity $<5\%$ RH was found lower in the case of SiO_2 -PIB sensors prepared with larger SDA content, in the $15\% < \text{RH} < 85\%$ range these samples displayed higher local sensitivity (see **Figure S3**). These findings demonstrate the role of micro-, and mesoporosity (at constant pore size) on the humidity sensing response in different RH ranges. We also note the reproducibility of the herein fabricated humidity sensors, with samples made from identical recipes but different batches displaying consistent behaviour (see SI **Figure S6**).

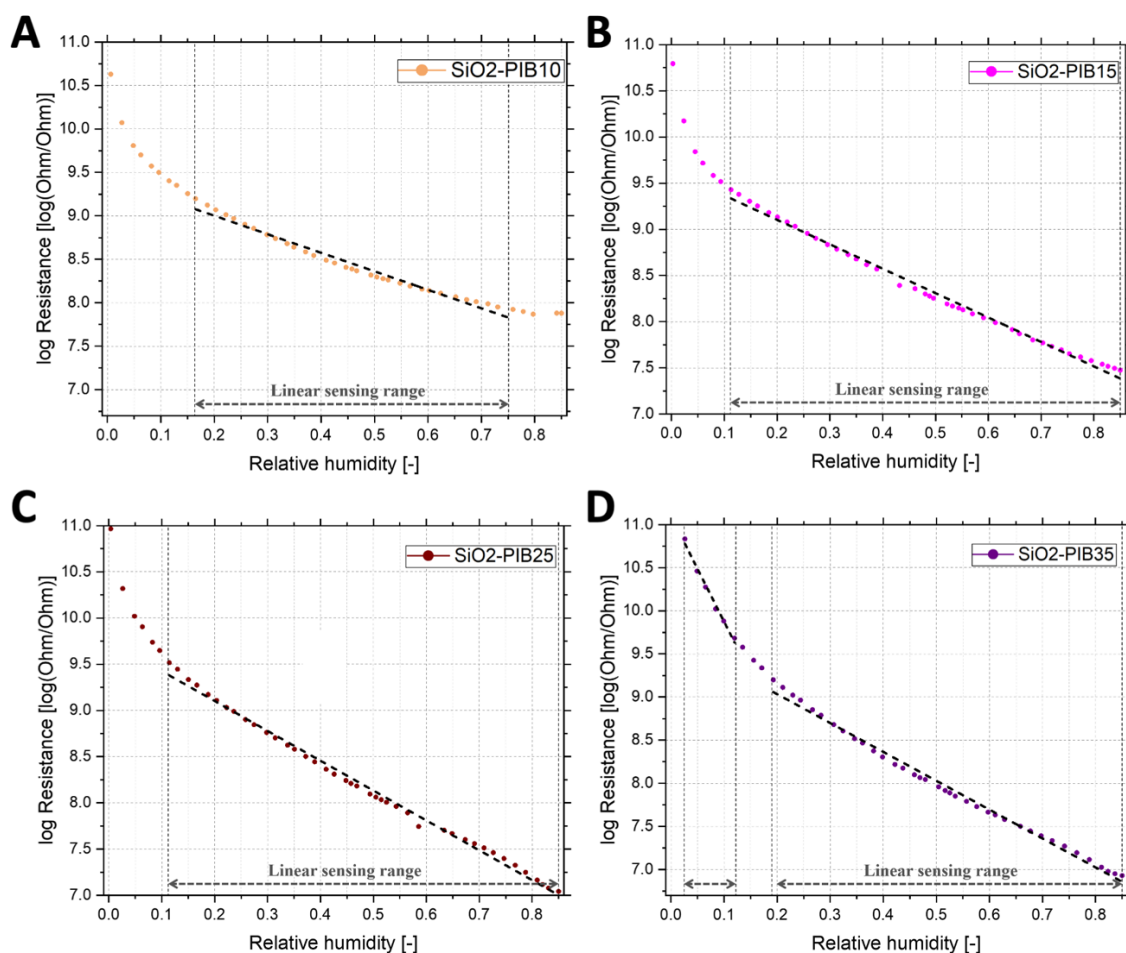


Figure 6. Sensitivity plots for adsorption of sensors SiO_2 -PIB10 (A), SiO_2 -PIB15 (B), SiO_2 -PIB25 (C) and SiO_2 -PIB35 (D) with linear fit in the linear sensing ranges identified

3.2.3.- Humidity sensing characteristics – influence of porosity on response/recovery times

The response/recovery behaviour of SiO_2 -PIB sensors are depicted in **Figure 7**. Sensors SiO_2 -PIB35, SiO_2 -PIB25, SiO_2 -PIB15 and SiO_2 -PIB10 showed monotonously increasing recovery times (9 s, 37 s, 53 s, 80 s). This trend is in line with the decrease in their meso-

and increase in their microporosities. It is worth noting, that the less microporous sensors SiO₂-CTAB and SiO₂-P also exhibited quicker recovery (7 s and 5 s respectively) than the more microporous SiO₂-PF (30 s), as discussed in chapter 3.1.3. All these results provide evidence of a correlation between microporosity in a sensing layer and slower recovery behaviour.

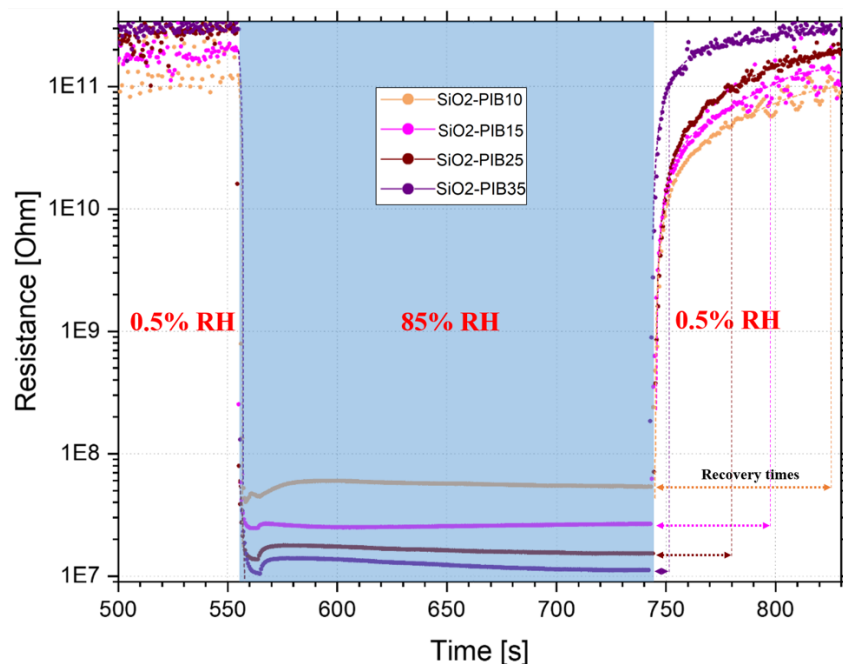


Figure 7. Response/recovery behaviour of SiO₂-PIB sensors

3.3 Sensor design guidelines: towards the optimal design.

The results discussed in the previous sections provide guidance towards the rational design of mesoporous sensors for desired sensitivity ranges. We attribute the main structural factors of porous architectures determining sensing behaviour to microporosity, mesoporosity, and pore size. Our findings are an extension to the pioneering work of K.-S. Chou et al. [77], who reported that specific surface area is the major contributor towards sensitivity at 10-20% RH, while porosity and capillary condensation plays the key role at higher RH (>80%).

Based on our analysis of the local sensitivity functions, the two sensors with the largest microporosity, templated by PF127 (SiO₂-PF) and 15% PIB-*b*-PEO (SiO₂-PIB15) were the most sensitive below 5% RH.

For applications operating in relatively narrow ranges of RH between 10% and 40%, CTAB-templated silica sensors (SiO₂-CTAB) offer higher performance and better linearity than the higher molecular weight block polymer-templated sensors investigated in this work (see **Figure 4**). The small (~3 nm) mesopores of SiO₂-CTAB were almost entirely filled up with water by 45% RH due to capillary condensation, which we relate as the cause of its high sensitivity in the lower RH range. This sensor also exhibited higher specific surface area than block copolymer-templated sensors (see **Table 2**).

The PEO-*b*-PPO-*b*-PEO templated sensors (SiO₂-P and SiO₂-PF) were found to be most sensitive between 35%-65% RH with good linearity, i.e. in the region where these sensors can take up the highest volume fraction of water in comparison to SiO₂-CTAB sensors, which have already reached their saturation water content and SiO₂-PIB sensors, where the larger mesopores adsorb smaller relative amounts of water (see **Figure 3**) in this range.

SiO₂-PIB sensors showcase good linearity in the 15%-65% range, furthermore their sensitivity can be significantly improved by increasing their porosity (SiO₂-PIB25 and SiO₂-PIB35 sensors). This increase in porosity corresponds to a larger pore volume where gradual multilayer adsorption can occur, resulting in a higher water uptake. This effect is visible in both EEP (**Figure 5**) and sensing response (**Figure 6**), which are in close correlation with each other. These sensors do not reach pore filling until 85% due to their larger pores (~15 nm), making them superior for sensing in the high RH (>65%) range while also offering best overall linearity in the widest RH range (15%-85%).

We want to emphasize on the role of microporosity for the response/recovery times. The less microporous sensors discussed in this work, SiO₂-CTAB, SiO₂-P and SiO₂-PIB35 are in-line or superior to the state of the art of silica-based humidity sensors within the last 5-10 years [32,33,78,79], while sensors with higher microporosity (e.g., SiO₂-PF and SiO₂-PIB15) exhibited slower response.

We further note that the sensor design guidelines presented in this paper for pure silica are applicable to other micro-/mesoporous matrices, which might be exploited due to the

inherent limitations of pure silica with regards to mechanical resistance [80] and long-term stability [81,82].

Table 2. Pore architectural parameters (obtained from EEP) of prepared sensors, and their response/recovery performance between 0.5% and 85%

<i>Sensor</i>	<i>Open Porosity (%)</i>	<i>Pore size (nm)</i>	<i>SSA (m²/cm³)</i>	<i>Response/Recovery times* (s)</i>
SiO₂-CTAB	48	3.1	1653	4/7
SiO₂-P	45	5.7	1379	3/5
SiO₂-PF	49	7.4	1027	4/30
SiO₂-PIB10	40	14.2	364	3/80
SiO₂-PIB15	46	14.8	382	3/53
SiO₂-PIB25	60	15.1	426	3/37
SiO₂-PIB35	70	16.0	552	3/9

*(between 0.5%-85% RH)

3 Conclusions

In summary, a series mesoporous silica resistive humidity sensors were fabricated using EISA with different SDAs. We found that for sensors with similar porosity ($47\pm 3\%$), pore size relates to the linear response range of the sensors. Sensors with larger pore size (~ 15 nm) showcased a wider linear response (15 to 85 % RH). The effect of porosity was also explored, with increased mesoporosity (to 60% or above) offering improved sensitivity and linearity, while increased microporosity providing improved performance at very low RH ($< 5\%$). Hence, we demonstrate that pore size and porosity are two key structural parameters in the performance of silica-based humidity sensors, with detailed tuning required for optimum operation across a target range. Future studies should aim to develop hierarchical architectures for optimum operation across the full RH range. We anticipate this work may guide application-specific cost-efficient manufacturing of commercial sensors and the development of ultra-high performance humidity sensors based on the discussed rationally designed structural characteristics.

Declaration of Competing Interest

The authors declare that they have no known competing financial interests or personal relationships that could have appeared to influence the work reported in this paper

Acknowledgments

M.F. is grateful for funding by an UCL Engineering Impact Studentship sponsored by Semilab Semiconductor Physics Laboratory Co. A.A.F., M.J.F., and S.G. acknowledge support by the EPSRC New Investigator Award (EP/R035105/1). The authors acknowledge Dr Ahmed Bentaleb and Dr Virginie Ponsinet (Université de Bordeaux, CNRS) for facility support and help with GISAXS measurements.

References

- [1] M. Srbinovska, C. Gavrovski, V. Dimcev, A. Krkoleva, V. Borozan, Environmental parameters monitoring in precision agriculture using wireless sensor networks, *J. Clean. Prod.* 88 (2015) 297–307. <https://doi.org/10.1016/j.jclepro.2014.04.036>.
- [2] R.N. Dean, A.K. Rane, M.E. Baginski, J. Richard, Z. Hartzog, D.J. Elton, A capacitive fringing field sensor design for moisture measurement based on printed circuit board technology, *IEEE Trans. Instrum. Meas.* 61 (2012) 1105–1112. <https://doi.org/10.1109/TIM.2011.2173041>.
- [3] N. Benabdellah, M. Bourhaleb, M. Nasri, N. Benazzi, S. Dahbi, Design of temperature and humidity sensors for an electronic nose used in rotten food, in: *Proc. 2016 Int. Conf. Electr. Inf. Technol.*, Institute of Electrical and Electronics Engineers Inc., 2016: pp. 505–509. <https://doi.org/10.1109/EITech.2016.7519652>.
- [4] J. Cai, C. Lv, E. Aoyagi, S. Ogawa, A. Watanabe, Laser Direct Writing of a High-Performance All-Graphene Humidity Sensor Working in a Novel Sensing Mode for Portable Electronics, *ACS Appl. Mater. Interfaces.* 10 (2018) 23987–23996.

<https://doi.org/10.1021/acsami.8b07373>.

- [5] B. Raju, R. Kumar, M. Senthilkumar, R. Sulaiman, N. Kama, S. Dhanalakshmi, Humidity sensor based on fibre bragg grating for predicting microbial induced corrosion, *Sustain. Energy Technol. Assessments*. 52 (2022) 102306. <https://doi.org/10.1016/J.SETA.2022.102306>.
- [6] B. Patissier, Humidity sensors for automotive, appliances and consumer applications, *Sensors Actuators B Chem*. 59 (1999) 231–234. [https://doi.org/10.1016/S0925-4005\(99\)00226-9](https://doi.org/10.1016/S0925-4005(99)00226-9).
- [7] S. Mondal, B.K. Min, Y. Yi, C.G. Choi, Highly Sensitive and Fast Responsive Humidity Sensor based on 2D PtSe₂ with Gamma Radiation Tolerance, *Adv. Mater. Technol*. 7 (2022). <https://doi.org/10.1002/ADMT.202100751>.
- [8] W.A. Jabbar, M.H. Alsibai, N.S.S. Amran, S.K. Mahayadin, Design and Implementation of IoT-Based Automation System for Smart Home, 2018 Int. Symp. Networks, Comput. Commun. ISNCC 2018. (2018). <https://doi.org/10.1109/ISNCC.2018.8531006>.
- [9] Y. Ma, S. Ma, T. Wang, W. Fang, Air-flow sensor and humidity sensor application to neonatal infant respiration monitoring, *Sensors Actuators A Phys*. 49 (1995) 47–50. [https://doi.org/10.1016/0924-4247\(95\)01014-R](https://doi.org/10.1016/0924-4247(95)01014-R).
- [10] M.A. Ryan, H. Zhou, M.G. Buehler, K.S. Manatt, V.S. Mowrey, S.P. Jackson, A.K. Kisor, A. V. Shevade, M.L. Homer, Monitoring space shuttle air quality using the jet propulsion laboratory electronic nose, *IEEE Sens. J*. 4 (2004) 337–347. <https://doi.org/10.1109/JSEN.2004.827275>.
- [11] S. Sikarwar, B.C. Yadav, Opto-electronic humidity sensor: A review, *Sensors Actuators A Phys*. 233 (2015) 54–70. <https://doi.org/10.1016/j.sna.2015.05.007>.
- [12] J. Wang, M.Y. Su, J.Q. Qi, L.Q. Chang, Sensitivity and complex impedance of nanometer zirconia thick film humidity sensors, *Sensors Actuators B Chem*. 139 (2009) 418–424. <https://doi.org/10.1016/j.snb.2009.03.070>.
- [13] Y. Sakai, M. Matsuguchi, T. Hুরুkawa, Humidity sensor using cross-linked poly(chloromethyl styrene), *Sensors Actuators B Chem*. 66 (2000) 135–138.

[https://doi.org/10.1016/S0925-4005\(00\)00313-0](https://doi.org/10.1016/S0925-4005(00)00313-0).

- [14] S. Mintova, S. Mo, T. Bein, Humidity sensing with ultrathin LTA-type molecular sieve films grown on piezoelectric devices, *Chem. Mater.* 13 (2001) 901–905.
<https://doi.org/10.1021/cm000671w>.
- [15] S. Muto, O. Suzuki, T. Amano, M. Morisawa, A plastic optical fibre sensor for real-time humidity monitoring, *Meas. Sci. Technol.* 14 (2003) 746–750.
<https://doi.org/10.1088/0957-0233/14/6/306>.
- [16] F. Gallego-Gómez, M. Morales, A. Blanco, C. López, Bare Silica Opals for Real-Time Humidity Sensing, *Adv. Mater. Technol.* 4 (2019) 1–10.
<https://doi.org/10.1002/admt.201800493>.
- [17] U. Kang, K.D. Wise, A high-speed capacitive humidity sensor with on-chip thermal reset, *IEEE Trans. Electron Devices.* 47 (2000) 702–710.
<https://doi.org/10.1109/16.830983>.
- [18] E. Zampetti, S. Pantalei, A. Pecora, A. Valletta, L. Maiolo, A. Minotti, A. Macagnano, G. Fortunato, A. Bearzotti, Design and optimization of an ultra thin flexible capacitive humidity sensor, *Sensors Actuators B Chem.* 143 (2009) 302–307.
<https://doi.org/10.1016/J.SNB.2009.09.004>.
- [19] K.P. Yoo, L.T. Lim, N.K. Min, M.J. Lee, C.J. Lee, C.W. Park, Novel resistive-type humidity sensor based on multiwall carbon nanotube/polyimide composite films, *Sensors Actuators B Chem.* 145 (2010) 120–125.
<https://doi.org/10.1016/j.snb.2009.11.041>.
- [20] G. Montesperelli, A. Pumo, E. Traversa, Gusmano, A. Bearzotti, A. Montenero, G. Gnappi, Sol-gel processed TiO₂-based thin films as innovative humidity sensors, *Sensors Actuators B Chem.* 25 (1995) 705–709. [https://doi.org/10.1016/0925-4005\(95\)85156-9](https://doi.org/10.1016/0925-4005(95)85156-9).
- [21] X. Le, Y. Liu, L. Peng, J. Pang, Z. Xu, C. Gao, J. Xie, Surface acoustic wave humidity sensors based on uniform and thickness controllable graphene oxide thin films formed by surface tension, *Microsystems Nanoeng.* 5 (2019) 1–10.

<https://doi.org/10.1038/s41378-019-0075-0>.

- [22] L. Alwis, T. Sun, K.T.V. Grattan, Optical fibre-based sensor technology for humidity and moisture measurement: Review of recent progress, *Measurement*. 46 (2013) 4052–4074. <https://doi.org/10.1016/j.measurement.2013.07.030>.
- [23] Y. Wang, Porous-Media Flow Fields for Polymer Electrolyte Fuel Cells: I. Low Humidity Operation, *J. Electrochem. Soc.* 156 (2009) B1124. <https://doi.org/10.1149/1.3183781>.
- [24] I. Fratoddi, A. Bearzotti, I. Venditti, C. Cametti, M. V. Russo, Role of nanostructured polymers on the improvement of electrical response-based relative humidity sensors, *Sensors Actuators B Chem.* 225 (2016) 96–108. <https://doi.org/10.1016/J.SNB.2015.11.001>.
- [25] S. Blessi, A. Manikandan, S. Anand, M.M.L. Sonia, V.M. Vinosel, A.M. Alosaimi, A. Khan, M.A. Hussein, A. M. Asiri, Enhanced electrochemical performance and humidity sensing properties of Al³⁺ substituted mesoporous SnO₂ nanoparticles, *Phys. E Low-Dimensional Syst. Nanostructures*. 133 (2021) 114820. <https://doi.org/10.1016/J.PHYSE.2021.114820>.
- [26] Y. Zhu, J. Chen, H. Li, Y. Zhu, J. Xu, Synthesis of mesoporous SnO₂–SiO₂ composites and their application as quartz crystal microbalance humidity sensor, *Sensors Actuators B Chem.* 193 (2014) 320–325. <https://doi.org/10.1016/J.SNB.2013.11.091>.
- [27] S.P. Gupta, A.S. Pawbake, B.R. Sathe, D.J. Late, P.S. Walke, Superior humidity sensor and photodetector of mesoporous ZnO nanosheets at room temperature, *Sensors Actuators B Chem.* 293 (2019) 83–92. <https://doi.org/10.1016/J.SNB.2019.04.086>.
- [28] V.K. Tomer, S. Duhan, A facile nanocasting synthesis of mesoporous Ag-doped SnO₂ nanostructures with enhanced humidity sensing performance, *Sensors Actuators B Chem.* 223 (2016) 750–760. <https://doi.org/10.1016/j.snb.2015.09.139>.
- [29] L. Almar, A. Tarancón, T. Andreu, M. Torrell, Y. Hu, G. Dezanneau, A. Morata, Mesoporous ceramic oxides as humidity sensors: A case study for gadolinium-doped ceria, *Sensors Actuators B Chem.* 216 (2015) 41–48.

- <https://doi.org/10.1016/j.snb.2015.04.018>.
- [30] T. Zhang, R. Wang, W. Geng, X. Li, Q. Qi, Y. He, S. Wang, Study on humidity sensing properties based on composite materials of Li-doped mesoporous silica A-SBA-15, *Sensors Actuators B Chem.* 128 (2008) 482–487.
<https://doi.org/10.1016/j.snb.2007.07.012>.
- [31] W. Geng, R. Wang, X. Li, Y. Zou, T. Zhang, J. Tu, Y. He, N. Li, Humidity sensitive property of Li-doped mesoporous silica SBA-15, *Sensors Actuators B Chem.* 127 (2007) 323–329. <https://doi.org/10.1016/j.snb.2007.04.021>.
- [32] V.K. Tomer, S. Duhan, Highly sensitive and stable relative humidity sensors based on WO₃ modified mesoporous silica, *Appl. Phys. Lett.* 106 (2015).
<https://doi.org/10.1063/1.4908116>.
- [33] W. Zhang, R. Wang, Q. Zhang, J. Li, Humidity sensitive properties of K-doped mesoporous silica SBA-15, *J. Phys. Chem. Solids.* 73 (2012) 517–522.
<https://doi.org/10.1016/j.jpcs.2011.10.030>.
- [34] T. Wagner, S. Krotzky, A. Weiß, T. Sauerwald, C.-D. Kohl, J. Roggenbuck, M. Tiemann, A High Temperature Capacitive Humidity Sensor Based on Mesoporous Silica, *Sensors.* (2011) 3135–3144. <https://doi.org/10.3390/s110303135>.
- [35] V.K. Tomer, S. Duhan, Nano titania loaded mesoporous silica: Preparation and application as high performance humidity sensor, *Sensors Actuators B Chem.* 220 (2015) 192–200. <https://doi.org/10.1016/j.snb.2015.05.072>.
- [36] X. He, W. Geng, B. Zhang, L. Jia, L. Duan, Q. Zhang, Ultrahigh humidity sensitivity of NaCl-added 3D mesoporous silica KIT-6 and its sensing mechanism, *RSC Adv.* 6 (2016) 38391–38398. <https://doi.org/10.1039/c6ra03385g>.
- [37] V.K. Tomer, S. Duhan, P. V. Adhyapak, I.S. Mulla, Mn-loaded mesoporous silica nanocomposite: A highly efficient humidity Sensor, *J. Am. Ceram. Soc.* 98 (2015) 741–747. <https://doi.org/10.1111/jace.13383>.
- [38] A. Bearzotti, J.M. Bertolo, P. Innocenzi, P. Falcaro, E. Traversa, Humidity sensors based on mesoporous silica thin films synthesised by block copolymers, *J. Eur. Ceram. Soc.* 24

- (2004) 1969–1972. [https://doi.org/10.1016/S0955-2219\(03\)00521-1](https://doi.org/10.1016/S0955-2219(03)00521-1).
- [39] J. Shah, R.K. Kotnala, B. Singh, H. Kishan, Microstructure-dependent humidity sensitivity of porous MgFe₂O₄-CeO₂ ceramic, *Sensors Actuators B Chem.* 128 (2007) 306–311. <https://doi.org/10.1016/j.snb.2007.06.021>.
- [40] F. Ernsberger, The Nonconformist Ion, *J. Am. Ceram. Soc.* 66 (1983) 747–750.
- [41] E.J. Connolly, G.M. O'Halloran, H.T.M. Pham, P.M. Sarro, P.J. French, Comparison of porous silicon, porous polysilicon and porous silicon carbide as materials for humidity sensing applications, in: *Sensors Actuators A Phys.*, Elsevier, 2002: pp. 25–30. [https://doi.org/10.1016/S0924-4247\(01\)00885-8](https://doi.org/10.1016/S0924-4247(01)00885-8).
- [42] G. Korotcenkov, E. Rusu, How to Improve the Performance of Porous Silicon-Based Gas and Vapor Sensors? Approaches and Achievements, *Phys. Status Solidi Appl. Mater. Sci.* 216 (2019) 1–30. <https://doi.org/10.1002/pssa.201900348>.
- [43] K. Sharma, S.S. Islam, Optimization of porous anodic alumina nanostructure for ultra high sensitive humidity sensor, *Sensors Actuators B Chem.* 237 (2016) 443–451. <https://doi.org/10.1016/j.snb.2016.06.041>.
- [44] Y. Pang, J. Jian, T. Tu, Z. Yang, J. Ling, Y. Li, X. Wang, Y. Qiao, H. Tian, Y. Yang, T.L. Ren, Wearable humidity sensor based on porous graphene network for respiration monitoring, *Biosens. Bioelectron.* 116 (2018) 123–129. <https://doi.org/10.1016/j.bios.2018.05.038>.
- [45] D. Grosso, F. Cagnol, G. Soler-Illia, E.L. Crepaldi, H. Amenitsch, A. Brunet-Bruneau, A. Bourgeois, C. Sanchez, Fundamentals of Mesostructuring Through Evaporation-Induced Self-Assembly, *Adv. Funct. Mater.* (2004) 309–322. <https://doi.org/10.1002/adfm.200305036>.
- [46] M. Stefik, J. Song, H. Sai, S. Guldin, P. Boldrighini, M.C. Orilall, U. Steiner, S.M. Gruner, U. Wiesner, Ordered mesoporous titania from highly amphiphilic block copolymers: Tuned solution conditions enable highly ordered morphologies and ultra-large mesopores, *J. Mater. Chem. A.* 3 (2015) 11478–11492. <https://doi.org/10.1039/c5ta02483h>.

- [47] P.C.A. Alberius, K.L. Frindell, R.C. Hayward, E.J. Kramer, G.D. Stucky, B.F. Chmelka, General predictive syntheses of cubic, hexagonal, and lamellar silica and titania mesostructured thin films, *Chem. Mater.* 14 (2002) 3284–3294. <https://doi.org/10.1021/cm011209u>.
- [48] E.L. Crepaldi, G.J. d. A.A. Soler-Illia, D. Grosso, F. Cagnol, F. Ribot, C. Sanchez, Controlled formation of highly organized mesoporous titania thin films: From mesostructured hybrids to mesoporous nanoanatase TiO₂, *J. Am. Chem. Soc.* 125 (2003) 9770–9786. <https://doi.org/10.1021/ja030070g>.
- [49] M. Nedelcu, J. Lee, E.J.W. Crossland, S.C. Warren, M.C. Orilall, S. Guldin, S. Hüttner, C. Ducati, D. Eder, U. Wiesner, U. Steiner, H.J. Snaith, Block copolymer directed synthesis of mesoporous TiO₂ for dye-sensitized solar cells, *Soft Matter*. 5 (2009) 134–139. <https://doi.org/10.1039/b815166k>.
- [50] H.N. Lokupitiya, A. Jones, B. Reid, S. Guldin, M. Stefik, Ordered Mesoporous to Macroporous Oxides with Tunable Isomorphic Architectures: Solution Criteria for Persistent Micelle Templates, *Chem. Mater.* 28 (2016) 1653–1667. <https://doi.org/10.1021/acs.chemmater.5b04407>.
- [51] A. Alvarez-Fernandez, M.J. Fornerod, B. Schmidt-hansberg, Fractionation of block copolymers for pore size control and reduced dispersity in mesoporous inorganic thin films†, *Nanoscale*. 12 (2020) 18455–18462. <https://doi.org/10.1039/d0nr05132b>.
- [52] H. Zhao, T. Zhang, R. Qi, J. Dai, S. Liu, T. Fei, G. Lu, Organic-inorganic hybrid materials based on mesoporous silica derivatives for humidity sensing, *Sensors Actuators B Chem.* 248 (2017) 803–811. <https://doi.org/10.1016/j.snb.2016.11.104>.
- [53] P. Innocenzi, A. Martucci, M. Guglielmi, A. Bearzotti, E. Traversa, Electrical and structural characterisation of mesoporous silica thin films as humidity sensors, in: *Sensors Actuators B Chem.*, Elsevier, 2001: pp. 299–303. [https://doi.org/10.1016/S0925-4005\(01\)00590-1](https://doi.org/10.1016/S0925-4005(01)00590-1).
- [54] V.K. Tomer, P. V. Adhyapak, S. Duhan, I.S. Mulla, Humidity sensing properties of Ag-loaded mesoporous silica SBA-15 nanocomposites prepared via hydrothermal process,

- Microporous Mesoporous Mater. 197 (2014) 140–147.
<https://doi.org/10.1016/j.micromeso.2014.06.007>.
- [55] S. Jakhar, S. Duhan, S. Nain, Facile hydrothermal synthesis of mesoporous WO₃ /KIT-6 nanocomposite depicting great humidity sensitive properties, Mater. Res. Innov. 26 (2022) 203–213. <https://doi.org/10.1080/14328917.2021.1940668>.
- [56] M. Groenewolt, T. Brezesinski, H. Schlaad, M. Antonietti, P.W. Groh, B. Ivan, Polyisobutylene-block-Poly(ethylene oxide) for Robust Templating of Highly Ordered Mesoporous Materials, Adv. Mater. 17 (2005) 1158–1162.
<https://doi.org/10.1002/adma.200401549>.
- [57] S. Guldin, S. Hüttner, P. Tiwana, M.C. Orilall, B. Ülgüt, M. Stefik, P. Docampo, M. Kolle, G. Divitini, C. Ducati, S.A.T. Redfern, H.J. Snaith, U. Wiesner, D. Eder, U. Steiner, Improved conductivity in dye-sensitised solar cells through block-copolymer confined TiO₂ crystallisation, Energy Environ. Sci. 4 (2011) 225–233.
<https://doi.org/10.1039/c0ee00362j>.
- [58] M. Matheron, T. Gacoin, J.P. Boilot, Stabilization of well-organized transient micellar phases in CTAB-templated silica and organosilica thin films, Soft Matter. 3 (2007) 223–229. <https://doi.org/10.1039/b612408a>.
- [59] Y. Yang, J. Li, H. Yuan, R. Carlini, X. Liu, The synthesis of mesoporous silica film using multi-templates directing and the effects of inorganic acids, Mater. Chem. Phys. 280 (2022) 125808. <https://doi.org/10.1016/j.matchemphys.2022.125808>.
- [60] C. Boissiere, D. Grosso, S. Lepoutre, L. Nicole, A.B. Bruneau, C. Sanchez, Porosity and mechanical properties of mesoporous thin films assessed by environmental ellipsometric porosimetry, Langmuir. 21 (2005) 12362–12371. <https://doi.org/10.1021/la050981z>.
- [61] A. Alvarez-Fernandez, B. Reid, M.J. Fornerod, A. Taylor, G. Divitini, S. Guldin, Structural Characterization of Mesoporous Thin Film Architectures: A Tutorial Overview, ACS Appl. Mater. Interfaces. 12 (2020) 5195–5208.
<https://doi.org/10.1021/acsami.9b17899>.
- [62] S. Brunauer, P.H. Emmett, The Use of Low Temperature van der Waals Adsorption

- Isotherms in Determining the Surface Areas of Various Adsorbents, *J. Am. Chem. Soc.* 59 (1937) 2682–2689. <https://doi.org/10.1021/ja01291a060>.
- [63] M. Thommes, K. Kaneko, A. V. Neimark, J.P. Olivier, F. Rodriguez-Reinoso, J. Rouquerol, K.S.W. Sing, Physisorption of gases, with special reference to the evaluation of surface area and pore size distribution (IUPAC Technical Report), *Pure Appl. Chem.* 87 (2015) 1051–1069. <https://doi.org/10.1515/pac-2014-1117>.
- [64] D. Babonneau, FitGISAXS: software package for modelling and analysis of GISAXS data using IGOR Pro, *J. Appl. Cryst.* 43 (2010) 929–936. <https://doi.org/10.1107/S0021889810020352>.
- [65] J. Loizillon, B. Baumgartner, C. Sinturel, M. Abbarchi, B. Lendl, D. Grosso, In-Depth Study of Coating Multimodal Porosity Using Ellipsometry Porosimetry in Desorption Scanning Mode, *J. Phys. Chem. C.* 123 (2019) 23464–23479. <https://doi.org/10.1021/acs.jpcc.9b05099>.
- [66] T. Galy, M. Marszewski, S. King, Y. Yan, S.H. Tolbert, L. Pilon, Comparing methods for measuring thickness, refractive index, and porosity of mesoporous thin films, *Microporous Mesoporous Mater.* 291 (2020). <https://doi.org/10.1016/j.micromeso.2019.109677>.
- [67] S. Kunchakara, M. Dutt, A. Ratan, J. Shah, V. Singh, Synthesis and characterizations of highly ordered KCl – MCM – 41 porous nanocomposites for impedimetric humidity sensing, *J. Porous Mater.* 26 (2019) 389–398. <https://doi.org/10.1007/s10934-018-0613-4>.
- [68] S. Dahiya, A. Kumar, S. Duhan, M.S. Goyat, Single-pot hydrothermal derived TiO₂ / SBA-16 cubic mesoporous nanocomposite for humidity sensing, *J. Mater. Sci.* 57 (2022) 3441–3451. <https://doi.org/10.1007/s10853-021-06822-0>.
- [69] M. Pi, D. Wu, J. Wang, K. Chen, J. He, J. Yang, D. Zhang, S. Chen, X. Tang, Real-time and ultrasensitive humidity sensor based on lead-free Cs₂SnCl₆ perovskites, *Sensors Actuators B Chem.* 354 (2022) 131084. <https://doi.org/10.1016/j.snb.2021.131084>.
- [70] J. Zhu, N. Zhang, Y. Yin, B. Xu, W. Zhang, C. Wang, High-Sensitivity and Low-

- Hysteresis GO-NH₂/Mesoporous SiO₂ Nanosphere-Fabric-Based Humidity Sensor for Respiratory Monitoring and Noncontact Sensing, *Adv. Mater. Interfaces*. 2101498 (2022) 1–11. <https://doi.org/10.1002/admi.202101498>.
- [71] X. Wang, J. hong Li, Y. Li, L. Liu, W. Guan, Emulsion-templated fully three-dimensional interconnected porous titania ceramics with excellent humidity sensing properties, *Sensors Actuators B Chem.* 237 (2016) 894–898. <https://doi.org/10.1016/j.snb.2016.07.014>.
- [72] P. Innocenzi, P. Falcaro, J.M. Bertolo, A. Bearzotti, H. Amenitsch, Electrical responses of silica mesostructured films to changes in environmental humidity and processing conditions, *J. Non. Cryst. Solids*. 351 (2005) 1980–1986. <https://doi.org/10.1016/j.jnoncrysol.2005.05.015>.
- [73] N.A. Melosh, P. Lipic, F.S. Bates, F. Wudl, G.D. Stucky, G.H. Fredrickson, B.F. Chmelka, Molecular and mesoscopic structures of transparent block copolymer-silica monoliths, *Macromolecules*. 32 (1999) 4332–4342. <https://doi.org/10.1021/ma9817323>.
- [74] M. Imperor-Clerc, P. Davidson, A. Davidson, Existence of a microporous corona around the mesopores of silica-based SBA-15 materials templated by triblock copolymers, *J. Am. Chem. Soc.* 122 (2000) 11925–11933. <https://doi.org/10.1021/ja002245h>.
- [75] D. Grosso, A.R. Balkenende, P.A. Albouy, A. Ayrat, H. Amenitsch, F. Babonneau, Two-dimensional hexagonal mesoporous silica thin films prepared from block copolymers: Detailed characterization and formation mechanism, *Chem. Mater.* 13 (2001) 1848–1856. <https://doi.org/10.1021/cm001225b>.
- [76] L. Vradman, L. Titelman, M. Herskowitz, Size effect on SBA-15 microporosity, *Microporous Mesoporous Mater.* 93 (2006) 313–317. <https://doi.org/10.1016/j.micromeso.2006.03.014>.
- [77] K. Sen Chou, T.K. Lee, F.J. Liu, Sensing mechanism of a porous ceramic as humidity sensor, *Sensors Actuators B Chem.* 56 (1999) 106–111. [https://doi.org/10.1016/S0925-4005\(99\)00187-2](https://doi.org/10.1016/S0925-4005(99)00187-2).
- [78] V.K. Tomer, S. Duhan, A.K. Sharma, R. Malik, S.P. Nehra, S. Devi, One pot synthesis

of mesoporous ZnO-SiO₂ nanocomposite as high performance humidity sensor, *Colloids Surfaces A Physicochem. Eng. Asp.* 483 (2015) 121–128.

<https://doi.org/10.1016/j.colsurfa.2015.07.046>.

- [79] P. Qi, Z. Xu, T. Zhou, T. Zhang, H. Zhao, Study on a quartz crystal microbalance sensor based on chitosan-functionalized mesoporous silica for humidity detection, *J. Colloid Interface Sci.* 583 (2021) 340–350. <https://doi.org/10.1016/j.jcis.2020.09.029>.
- [80] B. Reid, I. Mane, F. Ahmed, M.J. Fornerod, M. Furedi, B. Schmidt-Hansberg, A. Alvarez-Fernandez, S. Guldin, Enhanced mechanical stability and scratch resistance of mesoporous aluminosilicate thin films, *Microporous Mesoporous Mater.* (2022). <https://doi.org/10.1016/j.micromeso.2022.112246>.
- [81] J.D. Bass, D. Grosso, C. Boissiere, E. Belamie, T. Coradin, C. Sanchez, Stability of mesoporous oxide and mixed metal oxide materials under biologically relevant conditions, *Chem. Mater.* 19 (2007) 4349–4356. <https://doi.org/10.1021/CM071305G>.
- [82] S. Alberti, P.Y. Steinberg, G. Giménez, H. Amenitsch, G. Ybarra, O. Azzaroni, P.C. Angelomé, G.J.A.A. Soler-Illia, Chemical Stability of Mesoporous Oxide Thin Film Electrodes under Electrochemical Cycling: From Dissolution to Stabilization, *Langmuir.* 35 (2019) 6279–6287. <https://doi.org/10.1021/acs.langmuir.9b00224>.